

Smart Antennas for UTRA TDD

MARTIN HAARDT

Siemens AG, Information and Communication Mobile, Hofmannstr. 51, D-81359 Munich, Germany
haardt@ieee.org

CHRISTOPH F. MECKLENBRÄUKER

ftw. Telecommunications Research Center Vienna, Maderstr. 1/9, A-1040 Vienna, Austria
cfm@ieee.org

MARIUS VOLLMER

University of Dortmund, Information Processing Lab, D-44221 Dortmund, Germany
marius.vollmer@uni-dortmund.de

PETER SLANINA

Siemens AG Austria, PSE MCS Radio Access, A-1101 Vienna, Austria
peter.slanina@siemens.at

Abstract. Due to the increasing number of users in mobile communications and the demand for mobile multimedia services with high data rates, third generation mobile radio systems are currently one of the key communication technologies in research, development, and international standardization bodies. Smart antennas can be used to increase the capacity of wireless communication systems even further. TDD systems are particularly attractive for the employment of smart antennas, since the channel information (e.g., in terms of spatial covariance matrices) estimated on the uplink can be used directly for downlink beamforming. In this paper, we discuss efficient uplink and downlink processing techniques with smart antennas for UTRA TDD, the TDD mode of third generation mobile radio systems that is based on TD-CDMA. On the uplink, joint space-time processing is used to eliminate co-channel interference created by other users that transmit on the same frequency and in the same time slot. These joint detection techniques are efficiently implemented in the frequency domain. On the downlink, the data is only transmitted in the direction of the desired mobile user while interference in the direction of co-channel users is avoided. Moreover, *short-term* spatial channel estimates can be improved by projecting them into the dominant subspace of the *long-term* spatial covariance matrix. System level simulations have been performed to evaluate the gain in spectral efficiency (available bit rate per bandwidth per cell) if simple downlink beamforming techniques are used at the base stations. There is a two- to three-fold spectral efficiency gain if antenna arrays of $M = 8$ elements are deployed in a sectorized macro-cellular environment.

1 INTRODUCTION

In order to work towards a global third generation mobile radio standard, the Third Generation Partnership Project (3GPP, <http://www.3gpp.org/>) was formed in December 1998. 3GPP merged the already well harmonized proposals of the regional standardization bodies and continues to work on a common third generation mobile radio standard, which is called UMTS Terrestrial Radio Access (UTRA). UTRA is based on the evolved GSM core network and incorporates a frequency division duplex (FDD) as well as a time division duplex (TDD) mode [15]. More details about UTRA TDD can be found in [14].

Both modes of UTRA enable the implementation of smart antennas, where an antenna array at the base station is used for adaptive directional reception (on the uplink) and adaptive directional transmission (on the down-

link). Thereby, an increased antenna gain and an increased diversity gain are realized towards the desired user as illustrated in Figure 1. At the same time, less interference is received from the other directions (on the uplink) or transmitted in the other directions (on the downlink). Therefore, more users can be accommodated by the system and a corresponding increase of the spectral efficiency is achieved. On the uplink of UTRA TDD, joint detection and smart antenna techniques are combined via joint space-time processing schemes [2], [26]. Here, the intra-cell interference is eliminated via joint detection in the space-time domain. Moreover, the fact that the base stations of UTRA TDD are frame-synchronized facilitates the suppression of dominant co-channel interferers from adjacent cells (inter-cell interference) via smart antennas.

Due to the fact that the uplink and the downlink of TDD systems operate on the same frequency, channel parameters

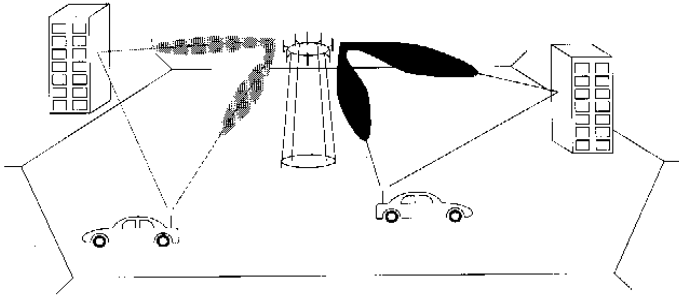


Figure 1: Smart antennas at the base station of a mobile radio system illustrated for two co-channel users.

(spatial covariance matrices) estimated on the uplink can also be used to calculate the weights for downlink beam-forming techniques.

Nevertheless, the interference situation can differ on the uplink and the downlink. This is particularly important if asymmetric services are considered. The sets of active users are defined dynamically by the scheduling and channel-allocation algorithms and need not be related. Here, we propose to use signaling over the network to inform adjacent cells about the sets of active users associated to particular time slots. If, however, such signaling is infeasible, then an *a priori* downlink covariance matrix can be used instead of an estimated one. A suitable *a priori* choice is based on omnidirectional plane waves carrying incoherent signals.

It was anticipated in the TSUNAMI II project that UMTS services can be seen as an evolution of the second generation GSM/DCS-1800 systems [19]. On the downlink, the antenna weights are chosen to maximize the transmitted power towards the desired mobile [23, 19]. It was predicted that the load factor on super reuse frequencies can be increased from approximately 30 % (interference limited) to potentially nearly 90 % (congestion limited) by deploying SFIR (spatial filtering for interference reduction) techniques, i.e., a load increase of a factor 2.5 can be achieved. In this context, a “reuse” factor of x % means that the frequency can be reused in adjacent cells in x % of the calls. For further details on these extrapolations, we refer to [23, 19]. In this paper, downlink system-level simulation results are presented for a TD-CDMA based system. The spectral efficiency results are in good agreement with the predictions and extrapolations in [23, 19].

The remainder of this paper is organized as follows. In Section 2 we discuss an efficient implementation of joint space-time processing schemes for the uplink of UTRA TDD. Then the downlink case is treated in Section 3. Implementation examples for the estimation of the required spatial covariance matrices are given in Section 4. After that, Section 5 addresses different ways of determining the spatial downlink covariance matrices in case of asymmetric traffic. In Section 6 some simulation results are summarized, before Section 7 concludes this paper.

2 UPLINK PROCESSING

2.1 FRAME STRUCTURE OF UTRA TDD

In the TD-CDMA system, K CDMA codes are simultaneously active on the same frequency and in the same time slot. The different spreading codes allow the signal separation at the receiver. According to the required data rate, a given user might use several CDMA codes and/or time slots. In Figure 2, the structure of one time slot is illustrated for the k -th midamble and the k -th spreading code. Here, Q denotes the spreading factor of the data symbols and N denotes the number of symbols in one data block. In this paper, we assume that all users use the same spreading factor. However, it is straightforward to extend the algorithms to variable spreading factors.

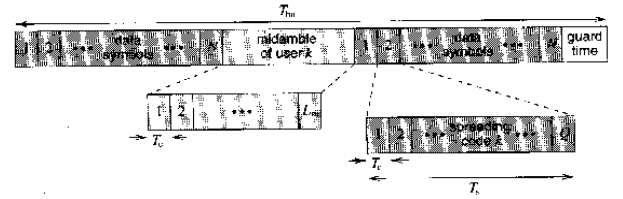


Figure 2: Time slot structure of the TD-CDMA system. Here, T_{bu} , T_s , T_c , and Q denote the burst duration, the symbol duration, the chip duration, and the spreading factor of the data symbols, respectively.

2.2 UPLINK DATA MODEL

A detailed derivation of the uplink data model for UTRA TDD can be found in [26]. Ultimately, the reception of all co-channel users in one half-burst is expressed as a set of linear equations,

$$\mathbf{x} = \mathbf{T}\mathbf{d} + \mathbf{n}, \quad (1)$$

where

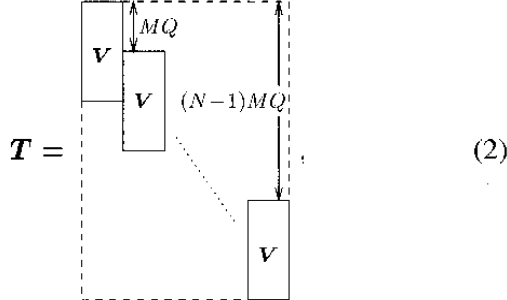
$$\mathbf{x} = \text{vec}\{\mathbf{X}\} \in \mathbb{C}^{M(NQ+W-1)}$$

and

$$\mathbf{d} = \text{vec}\{\mathbf{D}\} \in \mathbb{C}^{KN}.$$

Here, the vec -operator maps an $m \times n$ matrix into an mn -dimensional column vector by stacking the columns of the matrix, the $M \times (NQ + W - 1)$ matrix \mathbf{X} contains $NQ + W - 1$ samples from all M antennas at the base station, and the $K \times N$ matrix \mathbf{D} consists of N data symbols that were sent on the K simultaneously active CDMA codes. The parameter W denotes the maximum length of a channel impulse response. Moreover, the spatio-temporal vector $\mathbf{n} \in \mathbb{C}^{M(NQ+W-1)}$ in (1) models inter-cell interference, i.e., dominant interferers from adjacent cells, and additive (thermal) noise. The multiplication of \mathbf{d} by the system matrix \mathbf{T} represents the spreading of the data symbols and the influence of the individual multipath channels during transmission. The system matrix \mathbf{T} contains information about the spreading codes of each user and the estimated channel impulse responses.

The exact structure of \mathbf{T} depends on the order of the elements in the vectors \mathbf{x} and \mathbf{d} . Hence, there is some freedom in arranging the internal structure of \mathbf{T} . In order to find efficient algorithms for estimating \mathbf{d} from the knowledge of \mathbf{T} and \mathbf{x} , it is beneficial to work with band-structured block-Toeplitz matrices (also known as block-Sylvester matrices). The internal structure of \mathbf{T} is then given by



$$\mathbf{T} = \begin{bmatrix} \mathbf{V} & & \\ & \mathbf{V} & \\ & & \mathbf{V} \end{bmatrix} \quad (2)$$

i.e., \mathbf{T} consists of N identical copies of the block-matrix $\mathbf{V} \in \mathbb{C}^{M(Q+W-1) \times K}$, which in turn contains the spreading codes combined with the estimated channel impulse responses. More details about this data model can be found in [26].

2.3 JOINT DATA DETECTION VIA BLOCK LINEAR EQUALIZATION

The linear minimum variance unbiased estimate of the transmitted data symbols is given by [17]

$$\hat{\mathbf{d}} = \mathbf{W}^H \mathbf{x} = \left(\mathbf{T}^H \mathbf{R}_{nn}^{-1} \mathbf{T} \right)^{-1} \mathbf{T}^H \mathbf{R}_{nn}^{-1} \mathbf{x}, \quad (3)$$

where we assume that the space-time covariance matrix of the inter-cell-interference-plus-noise (IC-IN) $\mathbf{R}_{nn} = \frac{1}{M(NQ+W-1)} \mathbf{E}\{\mathbf{nn}^H\}$ is non-singular. In the literature, this solution is also called zero-forcing block linear equalizer. By estimating \mathbf{R}_{nn} , dominant interferers from adjacent cells can be suppressed.

If we assume that all the interfering wavefronts from adjacent cells originate from independent sources, the time correlations of the inter-cell multiple access interference are the same at each antenna element [29]. In this case, the space-time covariance matrix of the IC-IN can be expressed as the Kronecker product of the temporal covariance matrix of the IC-IN $\mathbf{R}_{I(t)}$ and the spatial covariance matrix of the IC-IN $\mathbf{R}_{I(s)}$, i.e., $\mathbf{R}_{nn} = \mathbf{R}_{I(t)} \otimes \mathbf{R}_{I(s)}$. This approximation facilitates the estimation of \mathbf{R}_{nn} by reducing its computational complexity. In UTRA TDD, $\mathbf{R}_{I(t)}$ can, furthermore, be approximated by the identity matrix. Hence, we only have to estimate the spatial covariance matrix of the IC-IN $\mathbf{R}_{I(s)}$.

Equation (3) can be efficiently computed by transforming it into the frequency domain [26]. Using the approximations for \mathbf{R}_{nn} outlined above along with the structure of \mathbf{T} described in (2), we can see that $\mathbf{S} = \mathbf{T}^H \mathbf{R}_{nn}^{-1} \mathbf{T}$ is a block-Toeplitz matrix. Similar to the schemes described in [26], \mathbf{S} can be approximated by a block-circular matrix.

Transforming this block-circular matrix into the frequency domain leads to a block-diagonal matrix, which can be efficiently inverted.

To actually compute \mathbf{S} , one has to consider the inverse of \mathbf{R}_{nn} . Using the approximations introduced above, we get

$$\mathbf{R}_{nn}^{-1} = \mathbf{I} \otimes \mathbf{R}_I^{-1}. \quad (4)$$

Equation (4) indicates that we only have to compute the inverse of the spatial covariance matrix of the IC-IN $\mathbf{R}_I \in \mathbb{C}^{M \times M}$. Hence, we can compute its Cholesky factor \mathbf{L}_I such that $\mathbf{L}_I^H \mathbf{L}_I = \mathbf{R}_I$. Then, we calculate the weighted system matrix $\tilde{\mathbf{T}}$ and the weighted right-hand side $\tilde{\mathbf{x}}$ via back substitution such that

$$\begin{aligned} \tilde{\mathbf{T}} &= (\mathbf{I} \otimes \mathbf{L}_I)^{-1} \mathbf{T}, \\ \tilde{\mathbf{x}} &= (\mathbf{I} \otimes \mathbf{L}_I)^{-1} \mathbf{x}. \end{aligned}$$

Note that $\tilde{\mathbf{T}}$ has the same block-Sylvester structure as the matrix \mathbf{T} in (2). Equation (3) can then be expressed as

$$\hat{\mathbf{d}} = \left(\tilde{\mathbf{T}}^H \tilde{\mathbf{T}} \right)^{-1} \tilde{\mathbf{T}}^H \tilde{\mathbf{x}}. \quad (5)$$

Another often used equalization criterion is the minimum mean square error (MMSE) criterion, which can be treated in a similar fashion.

2.4 EFFICIENT EQUALIZATION IN THE FREQUENCY DOMAIN

In this section, we describe the efficient computation of the the zero-forcing block linear equalizer (3) in the frequency domain. For notational simplicity, we will only refer to the system matrix \mathbf{T} (instead of $\tilde{\mathbf{T}}$), knowing that the incorporation of \mathbf{R}_{nn} into the equalization estimate does not influence the block-Sylvester structure of \mathbf{T} .

The *Block-Fourier* algorithm exploits the fact that the sampled baseband signals can be transformed efficiently to and from the frequency domain using Fast Fourier Transforms and that performing signal processing in the frequency domain is often more efficient than calculating the same task in the time domain. For example, it is well known that the convolution of two signals can be computed much more efficiently by transforming them to the frequency domain and performing element-wise multiplications there instead of a series of vector products in the time domain. The Block-Fourier algorithm is based on the same ideas as the fast convolution method: The received samples and the system matrix are transformed and the least squares solution is computed in the frequency domain. The final solution is then found by transforming the frequency solution back into the time domain.

Data Detection in the presence of a channel that is modeled by an FIR filter can be seen as the inverse problem to convolution, i.e., a deconvolution. Instead of multiplying the spectra element-wise in the frequency domain, we need to perform element-wise divisions. Just as in the convolution case, we must account for the fact that using a

discrete Fourier transform leads to a circular deconvolution. This can be realized by applying a suitable form of *zero-padding* and *overlapping* when constructing the solution from smaller parts, just as zero-padding and overlap-save or overlap-add is used in the fast convolution method. In the context of multi-user data detection, we face the additional problem that we need to extend the method to cope with the block-structure of the problem. This can be achieved by using *block-Fourier* transforms instead of the usual single signal transforms.

2.4.1 Diagonalizing block-circulant matrices

A circulant matrix is a square matrix where each column has the same elements as the column to the left of it, only rotated down by one position. By extension, a matrix is said to be block-circulant if the elements are not scalars but are themselves block-matrices. Since every block-matrix appears once in each block-column and in each block-row, all block-matrices must be of the same size.

Due to the fact that the Fourier vectors are the eigenvectors of circulant matrices, systems of equations with a circulant system matrix can be solved efficiently in the frequency domain. The transformation to and from the frequency domain is performed efficiently with Fast Fourier Transforms [13]. This well known scheme can be extended to block-circulant systems.

Block-circulant matrices can be block-diagonalized by block Fourier transforms. Suppose the block-circulant matrix C has blocks of size $P \times K$. Further, assume that C is of size $DP \times DK$, i.e., it has $D \times D$ blocks. Then we compute $\Lambda = F_{(P)} C F_{(K)}^{-1}$, where $F_{(P)}$ and $F_{(K)}$ are block Fourier transform matrices with block sizes of $P \times P$ and $K \times K$ respectively. They are defined as $F_{(n)} = F \otimes I_{(n)}$, where $I_{(n)}$ is the identity matrix of size $n \times n$, F is the Fourier matrix of size $D \times D$ and \otimes denotes the Kronecker product. The resulting matrix Λ will be block-diagonal, i.e., it is completely defined by its diagonal blocks of size $P \times K$. Similar to the scalar case, these block-matrices can be simply calculated via $F_{(P)} C(:, 1:K)$.

The properties of the block Fourier transform can be used to efficiently solve an equation like $Cd = x$ where C is block-circulant. Its LS solution $\hat{d} = C^+ x$ can be computed as

$$\hat{d} = F_{(K)}^{-1} \Lambda^+ F_{(P)} x, \quad (6)$$

where the superscript $+$ denotes the Moore-Penrose pseudo-inverse.

Thus, we need to apply a block Fourier transformation to x , then multiply by the pseudo-inverse of the block-diagonal matrix Λ and finally calculate an inverse block Fourier transform to get the result \hat{d} . Since Λ is block-diagonal, multiplying by its pseudo-inverse is in general significantly cheaper than using C directly.

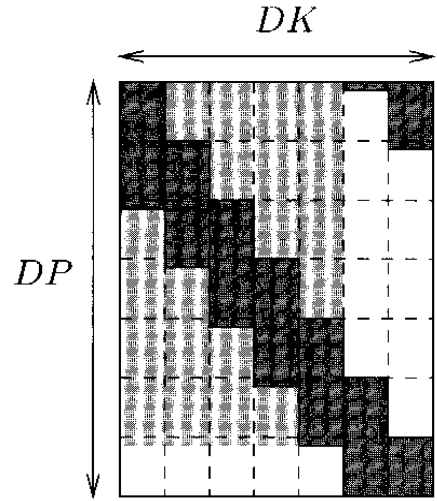


Figure 3: Extending the block-Sylvester matrix T (light shaded part) to be block-circulant.

2.4.2 Application to TD-CDMA

Although T is not block-square, the block-columns of T are already rotated versions of the first block-column. Therefore, we can simply add block columns to it until it is block-square. The number of block-columns that we must add depends on the degree of the block-band structure of T , which is the same as the inter-symbol interference in the original transmission system. Figure 3 shows how T can be extended to be block-circulant.

After T has been extended to be block-circulant, it has $D \times D$ blocks of size $P \times K$, where $D = N + \lceil (Q + W - 1)/Q \rceil - 1$ and $P = MQ$.¹ The vector x needs to be zero-padded at its end so that it has length DP . Likewise, the new solution vector contains the desired results in its first NK elements.

The simulations in Section 6 show that the error that occurs by solving for \hat{d} with this extended version of T is insignificant. This is due to the fact that the distortions introduced by extending T to be block-square affect only the guard periods between bursts. Neglecting the noise, the guard period between bursts facilitates it to model the channel correctly by a block-circulant matrix.

2.4.3 Overlap-save

The convolution matrix T with its strong band structure offers possibilities to reduce the computational demands of the joint detector even further. The idea is to reduce the size of the involved matrices and solve the whole problem by solving multiple smaller ones instead. The reduction in size is expressed by forcing D to smaller values when deriving a block-circular matrix from T according to Figure 3. With such a smaller matrix, only a smaller part of the data vector can be estimated. Thus, we need to partition the data vector into slices of length DK . But if D is smaller than its ideal value $N + \lceil (Q + W - 1)/Q \rceil - 1$, the

¹The notation $\lceil x \rceil$ denotes the *ceiling* of x , i.e., the smallest integer that is greater than or equal to x .

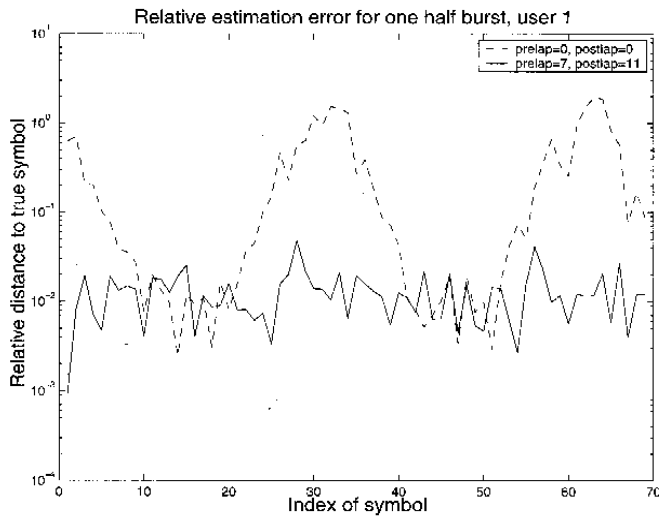


Figure 4: Estimation errors when using overlap-save techniques. $Q = 16$, $W = 57$, $N = 69$, $K = 4$, $M = 1$, $D = 32$, no noise.

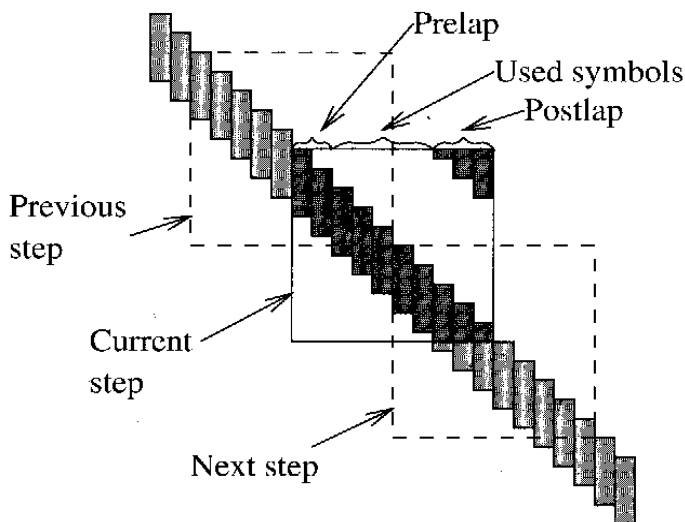


Figure 5: Overlapping Convolution Matrices with $D = 10$, $\text{prelap} = 2$, $\text{postlap} = 3$.

distortions mentioned in the previous section do no longer fall into the guard period, leading to unacceptable errors in the estimated data vector slices.

Figure 4 depicts this effect. The dashed line shows the relative error of the data symbols of one user, where D has been set to 32 and the full vector of $N = 69$ symbols has been calculated by carrying out the frequency domain detection three times on successive blocks of 32 symbols each. Obviously, each run of $D = 32$ symbols has large errors at the beginning and the end, but not in its middle part.

As a remedy, one discards a certain number of symbols at the start of the data vector slice (the *prelap*) and at the end of it (the *postlap*). The computation of the complete data vector needs to be arranged in such a way that the discarded symbols from the previous slice can be found in the middle

of the next one as depicted in Figure 5. Figure 4 shows that the relative error for such an overlapping computation has been reduced to a lower level for all symbols (solid line).

3 DOWNLINK PROCESSING

On the downlink, the spatial processing is carried out prior to transmission and, therefore, *before* the signal encounters the channel. This is very different from the uplink, where the spatial processing is performed *after* the channel has affected the signal. Therefore, it is possible to use blind or non-blind techniques on the received uplink signal to estimate the channel and/or the data. On the downlink, however, one either needs feedback of the signals received at the mobile station to get the channel information, or it may also be possible to determine the parameters of the downlink channel from the uplink. An excellent overview of uplink and downlink space-time processing for wireless communications has been presented in [21].

In the sequel, we only use spatial beamforming, i.e., space-only processing, at the base station, since there is also a temporal equalizer at the mobile station. The downlink spatial beamforming scheme should point beams in the direction of the desired user while minimizing the energy transmitted into the other directions as illustrated in Figure 1.

Assume that the base station uses an antenna array of M antennas to transmit K information signals to K different mobiles simultaneously. In TD-CDMA, the co-channel users share the same frequency and the same time slot but they can be separated by K different spreading codes. Let

$$\mathbf{w}^{(k)H} = \begin{bmatrix} w_1^{(k)} & w_2^{(k)} & \dots & w_M^{(k)} \end{bmatrix}, \quad (7)$$

$1 \leq k \leq K$, denote the beamforming vector of the k -th user that influences how the k -th transmitted signal couples into the channel as depicted in Figure 6. There are different strategies to determine the K spatial beamforming vectors $\mathbf{w}^{(k)}$.

Case 1

In the first approach [10, 6], the beamforming vectors are chosen such that the transmitted power $P_k = \mathbf{w}^{(k)H} \mathbf{w}^{(k)}$ is minimized subject to the constraint that a certain minimum signal-to-noise-plus-interference-ratio (SINR) is guaranteed at all K mobile stations.

Case 2

In [12], it is proposed to maximize the worst case signal quality at the K mobile stations. Here, the signal quality or signal-to-interference-ratio (SIR) is defined as the ratio of the time averaged signal power to the time averaged interference power.

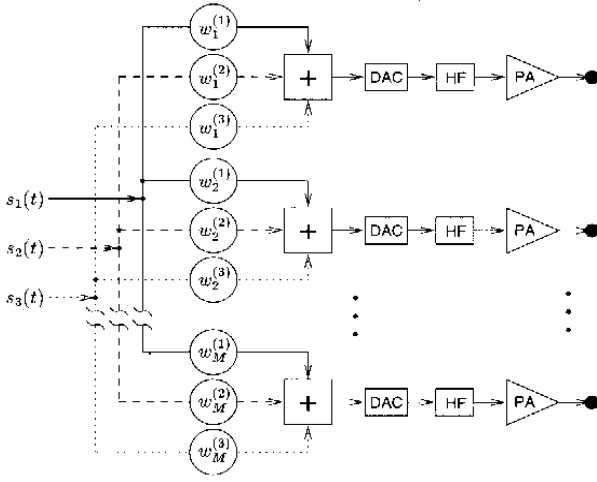


Figure 6: Downlink beamforming network illustrated for three co-channel users and M antennas. There is a digital-to-analog-converter (DAC), a high frequency (HF) converter, and a linear power amplifier (PA) at each antenna.

Case 3

Note that the solutions of case 1 and case 2 require iterative optimization procedures. It is, however, much simpler to minimize the interference generated to undesired users while maximizing the energy transmitted to the desired user. Then the expected value of the signal power received by the desired user k and created by the beamforming vector $\mathbf{w}^{(k)}$ is given by [10]

$$\mathbf{w}^{(k)H} \mathbf{R}_S^{(k)} \mathbf{w}^{(k)}, \quad (8)$$

where $\mathbf{R}_S^{(k)}$ denotes the spatial (downlink) covariance matrix of the k -th user. It incorporates the (medium-term) averaged spatial parameters that are equal on the uplink as well as the downlink.

The interference generated by the beamforming vector of the k -th user $\mathbf{w}^{(k)}$ towards other co-channel users may be expressed as

$$\mathbf{w}^{(k)H} \mathbf{R}_I^{(k)} \mathbf{w}^{(k)}. \quad (9)$$

Here, $\mathbf{R}_I^{(k)}$ denotes the spatial (downlink) covariance matrix of the set of co-channel users that interfere with user k . These co-channel users might be in the same cell and/or other (adjacent) cells of the network. If *joint detection* (or multi user detection) is applied on the downlink, i.e., at the mobiles, the co-channel interference caused by signals that are transmitted to *mobiles in the same cell* can be eliminated. Therefore, the spatial contributions of these mobiles are not incorporated into $\mathbf{R}_I^{(k)}$.²

In TDD systems, the uplink and downlink connections share the same carrier frequency by multiplexing the two directions in time. Therefore, the spatial covariance matrices estimated on the uplink can directly be used for the

²Thus, if joint detection is applied, the spatial covariance matrix $\mathbf{R}_I^{(k)} = \mathbf{R}_I$ only contains contributions from interfering co-channel mobiles from other cells.

downlink. These spatial covariance matrices may, for example, be estimated by exploiting the knowledge about the spreading codes, properties of the transmitted symbols, the transmitted training sequences, or a combination thereof. Hence, in TDD systems the estimation of the dominant directions of arrival is not required for downlink beamforming.

It is the goal of the described downlink beamforming scheme to find the beamforming vector $\mathbf{w}^{(k)}$ of the k -th user, $1 \leq k \leq K$, that maximizes the Rayleigh quotient

$$r(\mathbf{w}^{(k)}) = \frac{\mathbf{w}^{(k)H} \mathbf{R}_S^{(k)} \mathbf{w}^{(k)}}{\mathbf{w}^{(k)H} \mathbf{R}_I^{(k)} \mathbf{w}^{(k)}}. \quad (10)$$

It is given by the generalized eigenvector of the matrix pair $\mathbf{R}_S^{(k)}$ and $\mathbf{R}_I^{(k)}$ corresponding to its largest generalized eigenvalue $\lambda_{\max}^{(k)}$, i.e., it satisfies

$$\mathbf{R}_S^{(k)} \mathbf{w}^{(k)} = \mathbf{R}_I^{(k)} \mathbf{w}^{(k)} \lambda_{\max}^{(k)}.$$

The corresponding transmitted power equals

$$P_k = \mathbf{w}^{(k)H} \mathbf{w}^{(k)}$$

and should be adjusted via a traditional power control scheme such that the k -th user has an acceptable carrier to interference ratio. Alternatively, the powers can be adjusted by the base station(s) as described in [4].

4 ESTIMATION OF THE SPATIAL COVARIANCE MATRICES

In this section, we describe an efficient scheme of how the short-term spatial covariance matrices required for uplink and downlink processing may be estimated on the uplink. They are obtained by exploiting long-term and short-term spatial channel properties. The short-term spatial channel impulse responses can be estimated from the knowledge of the training sequence (midamble) in the current time slot. More sophisticated schemes (that may take into account decision feedback and forward error correction or other techniques to enhance the signal estimation accuracy) can, however, lead to an improved estimate as explained in [29].

In spatially correlated scenarios, improved (short-term) spatial channel estimates are obtained by projecting the current spatial channel estimates onto the subspace spanned by the dominant eigenvectors of the long-term spatial signal covariance matrix. This is particularly helpful in macro-cellular and micro-cellular environments. In this paper, we estimate the dominant subspace of the long-term spatial covariance matrix by averaging over all temporal taps of the channel impulse responses. The same strategy, however, can be applied to each temporal tap individually. The latter is advantageous if spatial characteristics differ substantially from tap to tap.

In a TD-CDMA based mobile radio system, the received signals are fed into a set of joint channel estimators. Assume that there is an antenna array of M antennas at the base station. Hence, the uplink channel impulse response matrix estimated for the k -th user in the i -th time slot

$$\begin{aligned} \mathbf{H}^{(k)}(i) &= \begin{bmatrix} \mathbf{h}_1^{(k)}(i) & \mathbf{h}_2^{(k)}(i) & \cdots & \mathbf{h}_W^{(k)}(i) \end{bmatrix} \\ &= \begin{bmatrix} \mathbf{h}^{(k,1)T}(i) \\ \mathbf{h}^{(k,2)T}(i) \\ \vdots \\ \mathbf{h}^{(k,M)T}(i) \end{bmatrix} \in \mathbb{C}^{M \times W}, \end{aligned} \quad (11)$$

$1 \leq k \leq K$, consists of M row vectors, each representing the discrete time channel impulse responses $\mathbf{h}^{(k,m)T}(i)$ of length W for the link between a certain user k and antenna m , $1 \leq m \leq M$. In adjacent cells of a cellular network, different midamble code sets with good cross-correlation properties should be used to guarantee a proper channel estimation.

Then an estimate of the long-term spatial covariance matrix of user k in the i -th time slot is given by

$$\begin{aligned} \mathbf{R}_S^{(k)}(i) &= \rho \mathbf{R}_S^{(k)}(i-1) + \frac{1-\rho}{W} \mathbf{H}^{(k)}(i) \mathbf{H}^{(k)H}(i) \quad (12) \\ &= \rho \mathbf{R}_S^{(k)}(i-1) + \frac{1-\rho}{W} \sum_{w=1}^W \mathbf{h}_w^{(k)}(i) \mathbf{h}_w^{(k)H}(i), \end{aligned}$$

$$\text{where } \mathbf{R}_S^{(k)}(0) = \frac{1}{W} \cdot \mathbf{H}^{(k)}(0) \mathbf{H}^{(k)H}(0)$$

and ρ is the forgetting factor ($0 \leq \rho \leq 1$).

Due to interference and additive noise, the spatial channel estimates will be noisy and $\mathbf{R}_S^{(k)}(i) \in \mathbb{C}^{M \times M}$ will have full rank M , if it is averaged over several time slots. The number of dominant paths L of the long-term spatial covariance matrix $\mathbf{R}_S^{(k)}(i)$ is equal to its number of dominant eigenvalues and could be determined via a simple threshold or via some information theoretic criteria, as for instance, described in [28]. Let $\mathbf{U}_s^{(k)} \in \mathbb{C}^{M \times L}$ contain the eigenvectors of the long-term spatial signal covariance matrix in the i -th time slot $\mathbf{R}_S^{(k)}(i)$ that correspond to its L largest eigenvalues.

In case of an FDD system, e.g., UTRA FDD, it is proposed in [5] to calculate the dominant long-term downlink eigenvectors $\mathbf{U}_s^{(k)}$ at the mobile station and to transmit them back to the base station on a long-term basis. Then only the "best" of these eigenbeams is selected at the mobile via short-term processing, its index is transmitted back to the base station, and it is used for downlink beamforming. In a TDD system, however, (as discussed in this paper) the long-term downlink spatial covariance matrix $\mathbf{R}_S^{(k)}(i)$ can be estimated on the uplink without the necessity for a frequency transformation.

In this paper, we do not (necessarily) select only one of these long-term eigenbeams for downlink beamforming, but choose the optimum combination of the columns of $\mathbf{U}_s^{(k)}$ to improve the accuracy of the short-term spatial

channel estimate significantly if the channel is spatially correlated. This is achieved by projecting a new short-term spatial channel estimate $\mathbf{H}^{(k)}(i) \in \mathbb{C}^{M \times W}$ onto the L -dimensional subspace spanned by the columns of $\mathbf{U}_s^{(k)}$, i.e.,

$$\begin{aligned} \hat{\mathbf{H}}^{(k)}(i) &= \mathbf{P}_s^{(k)} \cdot \mathbf{H}^{(k)}(i) \\ &= \mathbf{U}_s^{(k)} \left(\mathbf{U}_s^{(k)H} \mathbf{U}_s^{(k)} \right)^{-1} \mathbf{U}_s^{(k)H} \cdot \mathbf{H}^{(k)}(i). \end{aligned} \quad (13)$$

Note that the projector $\mathbf{P}_s^{(k)}$ simplifies to $\mathbf{P}_s^{(k)} = \mathbf{U}_s^{(k)} \mathbf{U}_s^{(k)H}$ if the columns of $\mathbf{U}_s^{(k)}$ are unitary. The estimation of $\hat{\mathbf{H}}^{(k)}(i)$ is illustrated in Figure 7 for $L = 2$. Based on the estimated channel impulse response matrix

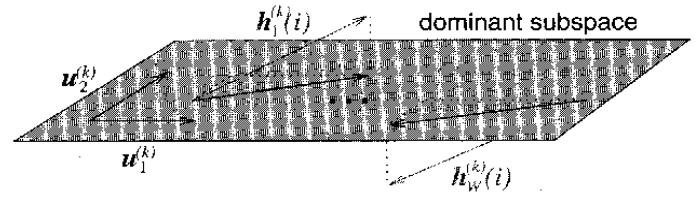


Figure 7: Illustration of how to project the short-term channel estimates $\mathbf{H}^{(k)}(i) = [\mathbf{h}_1^{(k)}(i) \cdots \mathbf{h}_W^{(k)}(i)]$ into the dominant subspace of the long-term spatial covariance matrix spanned by the columns of $\mathbf{U}_s^{(k)} = [\mathbf{u}_1^{(k)} \mathbf{u}_2^{(k)}]$. In this example, $L = 2$.

$\mathbf{H}^{(k)}(i)$, an improved short-time spatial covariance matrix at time i is obtained as

$$\hat{\mathbf{R}}_S^{(k)}(i) = \frac{1}{W} \cdot \mathbf{P}_s^{(k)} \mathbf{H}^{(k)}(i) \mathbf{H}^{(k)H}(i) \mathbf{P}_s^{(k)}. \quad (14)$$

Efficient updating schemes to track the projectors $\mathbf{P}_s^{(k)}$ from slot to slot have, for instance, been described in [25].

Next, the spatial covariance matrix of the signal-plus-interference-plus-noise $\mathbf{R}_{\text{SIN}} = \mathbb{E}\{\mathbf{x}(t)\mathbf{x}^H(t)\}$ is estimated. Here, $\mathbf{x}(t) \in \mathbb{C}^M$ denotes the noise and interference corrupted measurements at the base station antenna array. Let

$$\mathbf{X} = [\mathbf{x}(t_1) \mathbf{x}(t_2) \cdots \mathbf{x}(t_N)] \in \mathbb{C}^{M \times N}$$

contain the array measurements during one burst. Then a straightforward estimate of \mathbf{R}_{SIN} is given by

$$\mathbf{R}_{\text{SIN}} = \frac{1}{N} \cdot \mathbf{X} \mathbf{X}^H. \quad (15)$$

Especially for downlink applications, the estimates of the spatial covariance matrix \mathbf{R}_{SIN} should be averaged over several bursts using a rectangular or an exponential window.

If joint detection at the mobile (in case of downlink beamforming) or at the base station (in case of uplink interference cancellation) takes into account K co-channel signals, $\mathbf{R}_I^{(k)} = \mathbf{R}_I$ can be calculated as

$$\mathbf{R}_I = \mathbf{R}_{\text{SIN}} - \sum_{k=1}^K \hat{\mathbf{R}}_S^{(k)} \quad (16)$$

Note that (16) should be used for uplink processing as described in Section 2. On the other hand, if joint detection is not used, e.g., at the mobile terminal,

$$\mathbf{R}_1^{(k)} = \mathbf{R}_{\text{SIN}} - \mathbf{R}_S^{(k)}, \quad 1 \leq k \leq K. \quad (17)$$

5 DOWNLINK COVARIANCE MATRIX PREDICTION

The channel estimates $\mathbf{H}^{(k)}$ and \mathbf{X} required for evaluating equations (12) and (15) are performed at the base station during all uplink time slots. Note that the set of active users in a downlink time slot is not necessarily equal to the set of active users in any uplink time slot. Thus, the base station has to keep track of the active sets in uplink and downlink time slots by means of association tables that are updated via signaling over the network. Provided that the uplink/downlink time slot/user associations are known, the predicted downlink matrices equations (17) or (16) can be evaluated quite easily.

5.1 NETWORK MODEL

The base stations in adjacent cells are informed via signaling messages in the access network about the sets of active midamble codes in specific uplink and downlink time slots. The base stations use the signaled midamble sets for separating the interference contributions belonging to different users. This is necessary in general because the interference contributions must be *predicted* at the base station for the downlink time-slot at hand.

In a simpler approach, the uplink interference covariance matrix is estimated and used in the downlink, but this requires symmetric allocation of resources in the up- and downlink. Otherwise, the set of active users differ between the up- and downlink.

5.2 A PRIORI DOWNLINK SPATIAL COVARIANCE MATRICES

It might not be feasible to estimate the downlink spatial interference covariance matrices. Difficulties might arise from the instationarity of the channel, the implementational cost, or the complexity induced by the required network signaling. In such cases, it is possible to use an *a priori* chosen spatial covariance matrix. Such a covariance can be calculated from a probabilistic model of the interfering arrivals. In this section, we consider the special case of a uniform linear array with element spacing $\lambda/2$, because in this case the limiting form of the interference covariance matrices becomes particularly simple.

Spatially uncorrelated noise is not dominant in a mobile communications network. It is the interference from other mobile stations that accounts for most of the additive signal corruption. A simple spatial model can be formulated

by omnidirectional arrivals of plane waves with a uniform angular power density. For simplicity, the signals carried by these plane waves are assumed to be mutually uncorrelated in time. It is expected that this assumption is not too stringent, since the number of co-channel users is large whereas the number of correlated arrivals per user is much smaller. Moreover, it turns out that this model yields much better results than assuming spatially uncorrelated noise at all antennas. In a simple 2D model for the macro-cell environment, all users are distributed in a plane and their directions of arrival are uniformly distributed in azimuth along the unit circle at elevation 0° . Then the interference covariance matrix has Toeplitz structure and the individual elements are given by

$$[\mathbf{R}_I]_{mn} = J_0(\omega d_{mn}/c_0), \quad (18)$$

where $J_\ell(\cdot)$ denotes the Bessel function of the first kind and order ℓ .

In macro-cellular environments with 120° sectorization, it can be assumed that the directions of arrival are uniformly distributed in azimuth within the 120° sector at constant elevation 0° . Then the interference covariance matrix has the limiting form

$$[\mathbf{R}_I]_{mn} = 2\pi \sum_{\ell=-\infty}^{\infty} w_\ell J_\ell(\pi(m-n)), \quad (19)$$

where the coefficients w_ℓ are defined by

$$w_\ell = \begin{cases} 1/3, & \text{for } \ell = 0, \\ \frac{\sin(\pi\ell/3)}{\pi\ell}, & \text{else.} \end{cases} \quad (20)$$

A derivation of the series expansion (19) is provided in the appendix.

In micro-cellular and pico-cellular environments, the directions of arrival cannot be characterized by random arrivals in azimuth alone. The directions of arrival are distributed on the unit sphere. Often, a uniform distribution provides a suitable description. Whenever it is reasonable to model the interference plus noise wavefield as isotropic in three dimensions, the associated power spectral density is uniformly distributed over the solid angle 4π , i.e., on the unit sphere, and the spatial correlation is given by $\sin(\xi)/\xi$, where $\xi = \omega d/c_0$ and d is the distance between two observation locations of the wavefield, see [9] for details of the derivation and approximations. Hence, the associated covariance matrix can be modeled as

$$[\mathbf{R}_I]_{mn} = \sigma^2 \frac{\sin(\omega d_{mn}/c_0)}{\omega d_{mn}/c_0}. \quad (21)$$

The eigenvectors of this matrix are the Discrete Prolate Spheroidal Sequences (DPSS) [24].

6 SIMULATIONS

Performance of the joint detection schemes

Figure 8 compares the frequency domain implementation of the zero-forcing block linear equalizer for different overlapping degrees with the true least squares solution, obtained via a Cholesky factorization. The simulation scenario includes $K = 8$ users using one code each. To investigate the near/far resistance of the joint detector, four of these users have a power that is 20 dB above the remaining four users. This corresponds to a severe near/far scenario. The plotted bit error ratio is the mean of the four weaker users. Figure 8 shows that the presented joint detector is able to handle this critical situation better than the approximated Cholesky joint detector.

The label "C" in Figures 8 to 10 denotes the joint detector based on the Cholesky decomposition [3], "F" denotes the algorithm presented in this paper. "C exact" is the exact Cholesky decomposition and represents the true least squares solution. "C row" denotes a row-wise approximation of the Cholesky factors, where 2 block-rows have been computed [27]. It yields a slightly worse bit error ratio performance as "C exact". "C tri" uses the triangle approximation described in [18] with a sub-matrix of 2×2 blocks. It has a much worse performance than "C exact". The parameters for the Fourier algorithms are presented in the legend as $D/\text{prelap}/\text{postlap}$. The performance of the Fourier detector with no overlap ("F 128/0/0") is identical to the true least squares solution "C exact". When using significant overlap ("F 32/3/5"), the performance is still indistinguishable from "C exact", and with little overlap ("F 16/1/2") the performance is still comparable to "C row".

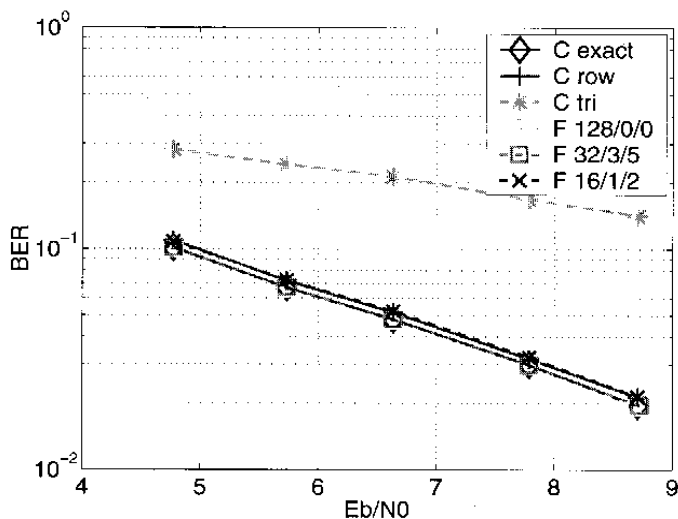


Figure 8: Bit error ratios after error correction of joint detection using different algorithms. The system parameters were chosen as $Q = 16$, $W = 57$, $N = 69$, $K = 8$, $M = 2$. The channel has been modeled as type Vehicular/A with a mobile velocity of 120 km/h. See the text for a discussion of the results.

Computational complexity

The additional processing requirements for computing \tilde{T} and \tilde{x} in Section 2 are modest. The number of real multiplications n is given by

$$n = \frac{2}{3}(M^3 - M) \quad (\text{Chol. dec.}) \\ + 2(vQK + NQ + W - 1)(M^2 - M) \quad (\text{back subst.}),$$

where $v = \lceil (Q + W - 1)/Q \rceil$. For example, a typical scenario with $Q = 16$, $K = 8$, $W = 57$, $N = 69$, $M = 8$ needs 201936 real multiplications, which amounts to about 11 % of the complete joint detection process. Figures 9 and 10 show the number of real multiplications needed for weighting along with the computational complexity required for the joint detection algorithms examined in [26] as a function of the number of active codes K and the number of antennas M , respectively.

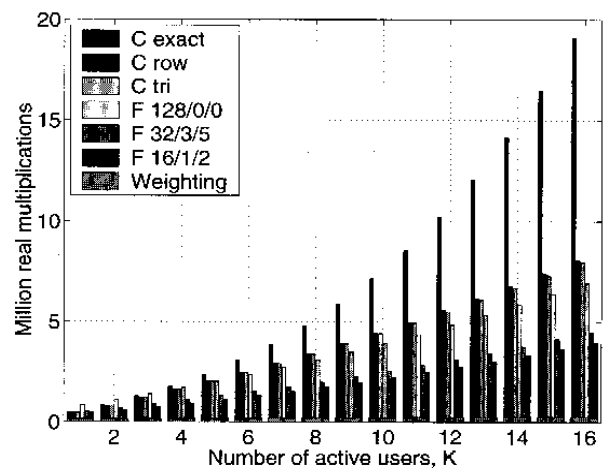


Figure 9: Computational complexity of the joint detection algorithms, as a function of the number of active codes K ($Q = 16$, $W = 57$, $N = 69$, $M = 8$).

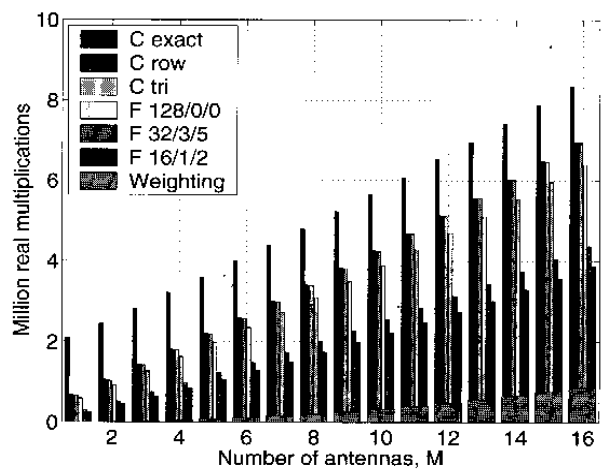


Figure 10: Computational complexity of the joint detection algorithms, as a function of the number of antennas M ($Q = 16$, $W = 57$, $N = 69$, $K = 8$).

Convergence of the rayleigh quotient

Downlink simulations are performed for evaluating the benefits from using the optimum weights \mathbf{w} that maximize (10). The simulation scenario consists of a base station equipped with a circular antenna array of $M = 8$ elements with $\lambda/2$ spacing. The signal of the user of interest is subject to multipath propagation (4 paths) with Laplace-distributed random angles and a standard deviation of 11° . The signal of the user of interest suffers from interference from $L \geq 1$ directions of arrival, which are uniformly distributed between 0° and 360° . All interfering signals have the same power. To keep the total power of the interference and the additive noise constant for all L , the power of the spatially uncorrelated (thermal) noise is decreased linearly with increasing L .

The resulting Rayleigh quotient $r(\mathbf{w}^{(k)})$ in (10) is averaged over 5000 Monte Carlo simulations. The results (in decibels) are plotted in Figure 11 (solid line). This performance is compared to the average performance of two sub-optimal weighting schemes. These reference schemes do not require an online estimation of \mathbf{R}_1 . The simplest approach uses the classical beamformer with weights \mathbf{b} obtained from maximizing (10) in case of spatially uncorrelated noise with $\mathbf{R}_1 = \sigma^2 \mathbf{I}$. The average Rayleigh quotient for the classical beamformer is also plotted in Figure 11 (dashed line). The third selected reference weighting vector \mathbf{v} uses the limit (18) of the spatial covariance matrix in case of a large number L of directions of arrival of the interference. The weighting vector \mathbf{v} is obtained as the dominant generalized eigenvector of the matrix pair $\mathbf{R}_S^{(k)}$ and \mathbf{R}_1 , where the elements of \mathbf{R}_1 are defined in (18). The convergence of the performance curve of the optimum beamformer \mathbf{w} to the one that assumes a large number of omnidirectional interferer \mathbf{v} is clearly visible in Figure 11. Thus, in rich scattering environments and/or in case of a large number of interferers, the performance of \mathbf{v} is close to that of \mathbf{w} .

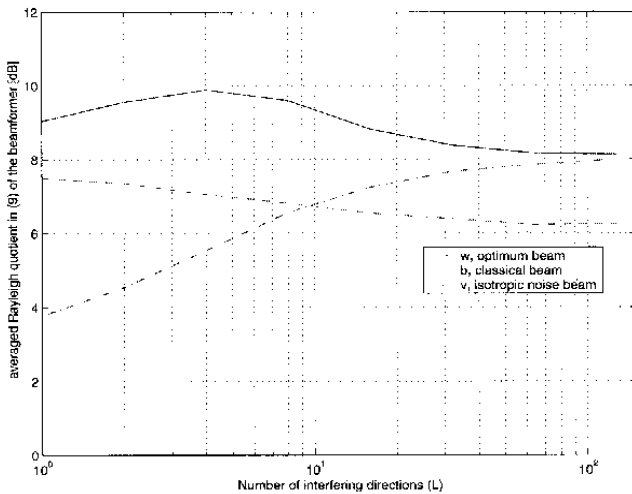


Figure 11: Plot of the average Rayleigh quotient as a function of the number of interfering wavefronts L .

Evaluation of downlink network throughput

System-level simulations were performed to evaluate the gain in network throughput for the *downlink* by means of beamforming at the base station transmitter and joint-detection in the mobile station receiver [7]. The system-level model is based on the sectorized “macro” environment specified in [1]. The model consists of a network with 19 sectorized sites with three sectors per site. This yields a total of 57 cells that contribute to the inter-cell interference. The traffic of the three innermost “reference” cells is evaluated to assess the performance of the network. All other cells serve as target cells for handover and contribute to the interference. This evaluation method ensures that the interference power in the reference cells is not under-estimated, cf. [20].

Joint detection is employed at the mobile stations to eliminate the intra-cell interference. The task of downlink beamforming is to reduce the remaining inter-cell interference; downlink notching of mobile stations in adjacent cells is not applied. The simulations are performed for a cellular network using circular arrays of $M = 8$ antennas with $\lambda/2$ -spacing at the base stations. The resulting idealized beampattern $B_0(\theta, 0^\circ)$ for the classical beamformer steered to 0° is shown in Figure 12 (dashed line).

In the simulations, it was assumed that the direction of arrival (DoA) statistics follow a Laplacian distribution with angular spread $S_\theta = 10^\circ = \pi/18$ rad. Instead of generating Laplacian distributed random angles during the runtime of the simulation, the following approach was adopted for reducing the run-time: For an individual user at a geometrical angle θ_0 relative to its base station, we can define the expected beampattern conditioned on θ_0

$$\begin{aligned} \bar{B}(\theta, \theta_0) &= \mathbb{E} \{ B(\theta - \theta_0, \theta_0) | \theta_0 \} \\ &= A \int_{-\pi}^{\pi} B_0(\theta - \theta_0, \theta_0) e^{-a|\theta|} d\theta \end{aligned}$$

where $a = \sqrt{2}/S_\theta$ and $A = [S_\theta(1 - e^{-a\pi})]^{-1}$. Thus, the system-level simulation was performed with the *expected* beampattern (with the main-lobe directed to the user of interest) rather than *random* realization. The smoothing operation is a circular convolution and evaluated efficiently via the FFT. The resulting smoothed beampattern $B(\theta, \theta_0)$ is shown in Figure 12 (solid line). The shape of the main-lobe is essentially unaffected by the smoothing, but considerable power leakage into the nulls of the ideal pattern is observed [7]. To reduce the run-time even further, the smoothed beampattern was approximated as rotationally invariant, i.e., the dependency of $\bar{B}(\theta - \theta_0, \theta_0)$ on the steering angle θ_0 was neglected. This is a good approximation for a uniform circular array. Finally, the smoothed beampattern was segmented into piece-wise constant angular intervals and stored in a ring-buffer during the simulations.

The receiver-side error statistics of the link-level simulator (which models the behavior of the physical layer) is entered into the system-level simulator via the “actual

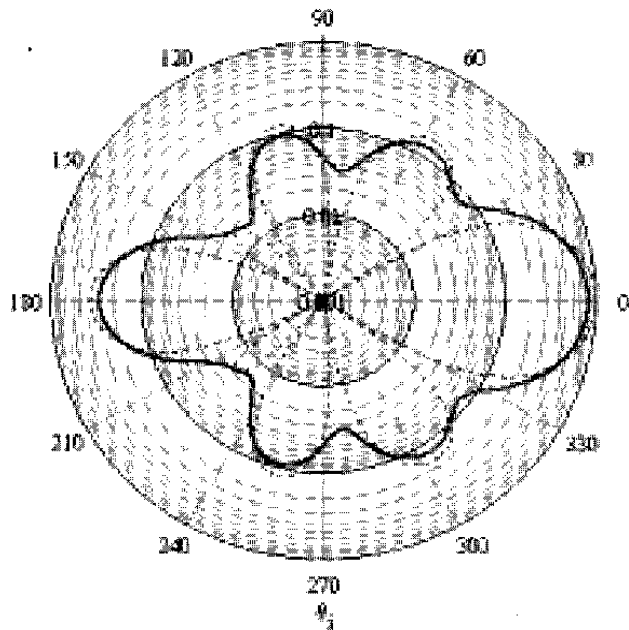


Figure 12: Ideal and smoothed beam patterns. Smoothing is performed for DoA spread $S_0 = 10^\circ$.

value interface" [16]. The simulated system employs a convolutional code with code-rate 0.3. Further details on the system-level simulation and the interfacing to link-level can be found in [7].

To evaluate the performance gain due to smart antennas, three scenarios were investigated: In the first two scenarios, channels were assigned randomly from a given set of channels (Fixed Channel Allocation, FCA), where power control was performed in the second scenario and disabled in the first scenario. In the third scenario, channels were assigned by selecting the "best" channel according to a specified optimization criterion (Dynamic Channel Allocation, DCA). The chosen DCA strategy was "Channel Segregation" using an interference threshold for the priority table [22]. Figure 13 shows the percentage of "satisfied" downlink speech users in a cell. User satisfaction is defined in [1] as a user enjoying a bit error rate lower than 10^{-3} (after decoding) for at least 95 % of the call duration. Furthermore the call must not get dropped due to a bit error rate exceeding 10^{-3} for more than 5 s. The user percentages are shown along the vertical axis and the horizontal axis depicts the load on a linear scale (bit rate per bandwidth per cell). The linear scale is normalized such that the maximum achieved network spectral efficiency without smart antennas is 100: This baseline value is achieved where the curve marked with \diamond crosses the required 98 % user satisfaction. The maximum spectral efficiency gain is achieved if the smart antennas are switched on. The spectral efficiency for smart antennas switched on, but without power control (line marker ∇ in Figure 13 and labeled as "FCA, PC off, SMA on") is even higher than the case where power control and DCA are both switched on, but without smart antennas (line marker \diamond). In the case of smart antennas switched on, an additional gain in spectral efficiency is achieved if

power control is used (lines marked with ∇ and \star). The contribution to the spectral efficiency gain of DCA is modest compared to power control (lines marked with \star and ∇). The spectral efficiency due to downlink beamforming alone is found by simulations to be approximately 55 % higher than the combined gain resulting from power control and DCA without beamforming. Note that the spectral efficiency resulting from power control and beamforming together is higher than the best system without beamforming by a factor of 2.63. Lastly, if DCA is used in conjunction with downlink beamforming and power control, the spectral efficiency reaches 2.67 times the baseline value. Thus, it is safe to say that there is no additional gain from DCA when power control and downlink beamforming are used together. In fact, the best spectral efficiency value is very close to the hard blocking limit. The optimized spectral efficiencies for these six system-level simulation scenarios are visualized in the bar-graph of Figure 14.

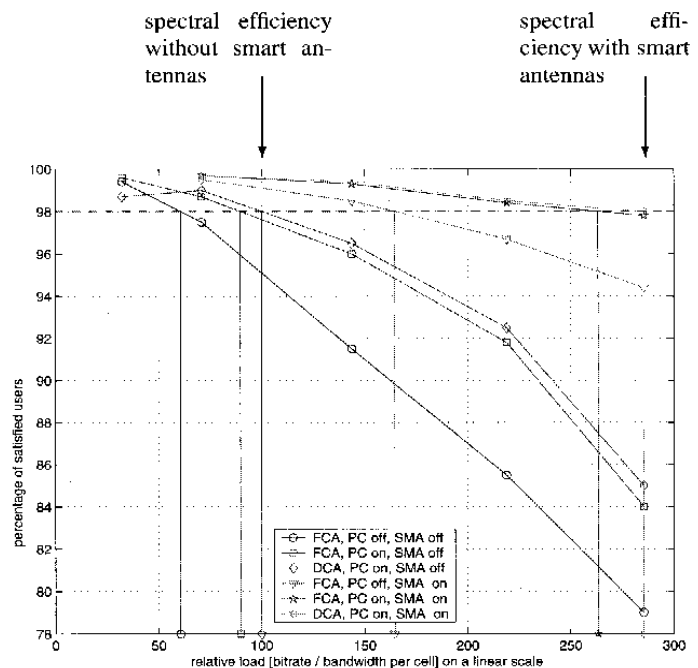


Figure 13: Percentage of satisfied users in the network. This percentage must not drop below 98 %, cf. [1].

7 CONCLUSIONS

In this paper, we have discussed smart antenna concepts for the uplink and the downlink of UTRA TDD. On the uplink, joint space-time processing schemes eliminate intra-cell interference and suppress inter-cell interference. They can be implemented efficiently in the frequency domain [26]. Here, we have shown how inter-cell interference can be suppressed and have presented formulas for the required computational complexity.

Moreover, we have described and compared several downlink beamforming schemes that are based on spatial covariance matrices estimated on the uplink. To avoid in-

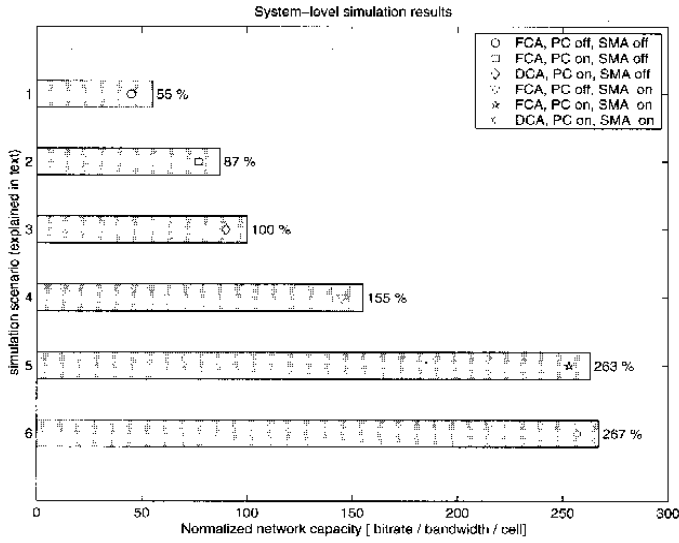


Figure 14: Spectral efficiency of the network for the six system-level deployment scenarios evaluated according to [1].

interference to inter-cell users that are active in the same time slot, it is proposed to use signaling over the network to inform adjacent cells about the sets of active midambles. Base stations can predict downlink covariance matrices for specific time slots using the signaled midamble sets. Alternatively, an omnidirectional interference model may be employed in a dense cellular network for pre-calculating an *a priori* downlink covariance matrix. The resulting beam-patterns have superior properties than the classical beam-patterns, which are calculated for the uncorrelated (spatially white) noise case.

Finally, from the system-level simulations for downlink speech traffic using beamforming at the network-side and joint-detection at the mobile stations, it is concluded that the gain in spectral efficiency due to downlink beamforming is approximately 55 % higher than the gain resulting from Power Control (PC) and Dynamic Channel Allocation (DCA) combined. With downlink beamforming and power control together, there is no additional gain from employing DCA. If downlink beamforming is used in conjunction with PC, the spectral efficiency reaches more than 2.6 times the spectral efficiency resulting from PC and DCA without downlink beamforming. The presented spectral efficiency improvements are achieved by antenna arrays of $M = 8$ elements.

APPENDIX

A brief derivation of the series expansion (19) is given here. It is assumed that the interference scenario is two-dimensional, i.e., the spread in elevation θ is negligible as compared to the spread in azimuth ϕ [11, 8]. Further, the

antenna array is assumed to be a horizontal planar array. In this case, the (n, m) -th element of the interference covariance matrix is given by [9]

$$R_{nm} = \int_{-\pi}^{\pi} w(\phi) \exp \left[j \frac{\omega}{c_0} d_{nm} \cos(\phi - \delta_{nm}) \right] d\phi, \quad (22)$$

where d_{nm} is the distance between the antenna array elements n and m . Moreover, δ_{nm} defines the orientation of the line which joins them. If the n -th array element has cartesian coordinates (x_n, y_n) , then d_{nm} and δ_{nm} are defined by

$$\begin{aligned} d_{nm} \cos \delta_{nm} &= x_n - x_m, \\ d_{nm} \sin \delta_{nm} &= y_n - y_m. \end{aligned}$$

In the special case of a horizontal linear array, it can be assumed that all differences $y_n - y_m$ vanish and $\delta_{nm} \in \{0, \pi\}$. The angular weighting function $w(\phi)$ describes the angular power distribution. Thus, $w(\phi) \geq 0$ for all $-\pi \leq \phi < \pi$ and $w(\phi)$ is periodic with period 2π . Now, let $w(\phi)$ be expandable in a Fourier series

$$w(\phi) = \sum_{\ell=-\infty}^{\infty} w_{\ell} e^{-j\ell\phi}, \quad \text{with } w_{\ell} = \frac{1}{2\pi} \int_{-\pi}^{\pi} w(\phi) e^{j\ell\phi} d\phi.$$

The Fourier series is inserted into (22) resulting in

$$R_{nm} = \sum_{\ell=-\infty}^{\infty} w_{\ell} \int_{-\pi}^{\pi} \exp \left(j \frac{\omega}{c_0} d_{nm} \cos(\phi - \delta_{nm}) - j\ell\phi \right) d\phi.$$

The remaining integral is recognized as $2\pi \exp(j\delta_{nm})$ -times the Bessel function $J_{\ell}(\cdot)$ of the first kind and order ℓ , which yields

$$R_{nm} = 2\pi \sum_{\ell} w_{\ell} e^{j\ell\delta_{nm}} J_{\ell} \left(\frac{\omega}{c_0} d_{nm} \right). \quad (23)$$

A sectorized macro-cellular environment with sectors of angular width 2β is described by the ideal rectangular power weighting function $w(\phi) = 0$ for $|\phi| > \beta$ and $w(\phi) = 1$ for $|\phi| < \beta$. In this case, the Fourier coefficients become

$$w_0 = \frac{\beta}{\pi}, \quad w_{\ell} = \frac{\sin(\beta\ell)}{\pi\ell} \quad (24)$$

This coincides with the result given in Section 5.2 for a linear horizontal antenna array in a sectorized environment with sectors of width $2\beta = 120^\circ$.

ACKNOWLEDGEMENTS

The work on this paper was supported partly by Siemens AG Germany, the Wiener Wirtschaftsförderungsfonds (WWFF), and Siemens AG Austria PSE PRO RCD

through the ftw. project C2 "Smart Antennas". The authors would also like to thank the reviewer for his constructive comments.

Manuscript received on June 1, 2001.

REFERENCES

- [1] ETSI TR 101 112. Selection procedures for the choice of radio transmission technologies of the universal mobile telecommunications system UMTS (UMTS 30.03), version 3.2.0. Apr. 1998.
- [2] P.W. Baier, A. Papathanassiou, and M. Weckerle. Recent results on the benefits of adaptive antennas in TD-CDMA mobile radio systems. In *Proc. IEEE / IEE Int. Conf. on Telecommunications*, Vol. 1, pages 399–404, Cheju, South Korea, June 1999.
- [3] J.J. Bantz, A. Klein, M. Naßhan, and A. Steil. Performance of a cellular hybrid C/TDMA mobile radio system applying joint detection and coherent receiver antenna diversity. *IEEE Journal on Selected Areas in Communications*, Vol. 12, pages 568–579, May 1994.
- [4] H. Boche and M. Schubert. A new approach to power adjustment for spatial covariance based downlink beamforming. In *Proc. IEEE Int. Conf. Acoust., Speech, Signal Processing*, Salt Lake City, UT, May 2001.
- [5] C. Brunner. *Efficient Space-Time Processing Schemes for WCDMA*, Ph. D. dissertation, Munich University of Technology, Munich, Germany, July 2000, Shaker Verlag, J.A. Nossek, editor.
- [6] C. Brunner, M. Joham, W. Utschick, M. Haardt, and J.A. Nossek. Downlink beamforming for WCDMA based on uplink channel parameters. In *Proc. 3rd European Personal Mobile Communications Conference (EPMCC '99)*, pages 375–380, Paris, France, Mar. 1999.
- [7] M. Bublin, G. Diernhofer, C.F. Mecklenbräuker, T. Patic, J. Plogsties, and P. Slanina. System-level simulation of smart antennas for 3G mobile systems using TD-CDMA. In *Proc. 4th European Personal Mobile Communications Conf. (EPMCC 2001)*, Vienna, Austria, Feb. 2001.
- [8] L.M. Correia, Ed. *Wireless Flexible Personalised Communications, COST 259: European Co-operation in Mobile Radio Research*. John Wiley and Sons, Mar. 2001.
- [9] B.F. Cron and C.H. Sherman. Spatial-correlation functions for various noise models. *Journal of the Acoustical Society of America*, Vol. 34, No. 11, pages 1732–1736, Nov. 1962.
- [10] C. Farsakh and J.A. Nossek. Spatial covariance based downlink beamforming in an SDMA mobile radio system. *IEEE Trans. Communications*, Vol. 46, pages 1497–1506, Nov. 1998.
- [11] B.H. Fleury. First- and second-order characterization of direction dispersion and space selectivity in the radio channel. *IEEE Transactions on Information Theory*, Vol. 46, No. 6, pages 2027–2044, Sept. 2000.
- [12] D. Gerlach and A. Paulraj. Base station transmitting antenna arrays for multipath environments. *Signal Processing*, Vol. 54, pages 59–73, 1996.
- [13] G.H. Golub and C.F. van Loan. *Matrix Computations*, Johns Hopkins University Press, Baltimore, MD, 3rd edition, 1996.
- [14] M. Haardt, A. Klein, R. Koehn, S. Oestreich, M. Purat, V. Sommer, and T. Ulrich. The TD-CDMA based UTRA TDD mode. *IEEE J. Select. Areas Commun.*, Vol. 18, pages 1375–1386, Aug. 2000, special issue on "Wideband CDMA".
- [15] M. Haardt and W. Mohr. The complete solution for third-generation wireless communications: Two modes on air, one winning strategy. *IEEE Personal Communications Magazine*, Vol. 7, No. 6, pages 18–24, Dec. 2000.
- [16] S. Haemaeläinen, P. Slanina, M. Hartman, A. Lappela, H. Holma, and O. Salonaho. A novel interface between link and system level simulations. In *ACTS Mobile Communications Summit '97*, pages 599–604, Aalborg, Denmark, Oct. 1997.
- [17] S. M. Kay. *Fundamentals of Statistical Signal Processing – Estimation Theory*. Prentice Hall, Englewood Cliffs, NJ, 1993.
- [18] J. Mayer, J. Schlee, and T. Weber. Realtime feasibility of joint detection CDMA. In *Proc. 2nd European Personal Mobile Communications Conference*, pages 245–252, Bonn, Germany, Sept. 1997.
- [19] P.E. Mogensen, P. Zetterberg, H. Dam, P. Leth-Espensen, and F. Frederiksen. Algorithms and antenna array recommendations (part I). Tech. Rep. CEC Deliverable AC020/AUC/A1.2/DR/P/005/b1, ACTS 020: Technology in Smart Antennas for Universal Advanced Mobile Infrastructure (Part 2), TSUNAMI (II), Oct. 1996.
- [20] T. Neubauer, T. Baumgartner, and E. Bonek. Necessary and sufficient network size for pole capacity estimation in UMTS FDD. In *European Conference on Wireless Technologies (ECWT 2000)*, Paris, France, Oct. 2000.
- [21] A. J. Paulraj and C. B. Papadias. Space-time processing for wireless communications. *IEEE Signal Processing Magazine*, pages 49–83, Nov. 1997.
- [22] R. Prasad, W. Mohr, and W. Konhäuser, Eds. *Third Generation Mobile Communication Systems*. Artech House Universal Personal Communications Series. Artech House Publishers, Boston and London, 2000.
- [23] R. Rheinschmitt and M. Tangemann. Performance of sectorised spatial multiplex systems. In *Proc. IEEE Vehicular Techn. Conf.*, Vol. 1, pages 426–430, Atlanta, GA, Apr. 1996.
- [24] D. Slepian. Prolate spheroidal wave functions, fourier analysis and uncertainty — part v: The discrete case. *Bell Systems Technical Journal*, Vol. 57, pages 1371–1429, 1978.
- [25] W. Utschick. Tracking of signal subspace projectors. Tech. Rep. TUM-LNS-TR-00-1, Munich University of Technology, Munich, Germany, 2000, also submitted to the *IEEE Trans. on Signal Processing*.
- [26] M. Vollmer, J. Götze, and M. Haardt. Efficient joint detection techniques in the frequency domain for third generation

- mobile radio systems. In *Proc. IEEE International Conf. on Third Generation Wireless Communications*, pages 623–630, San Francisco, CA, June 2000. Dclson Group.
- [27] M. Vollmer, M. Haardt, and J.Götze, Schur algorithms for joint detection in TD-CDMA based mobile radio systems. *Annales des Télécommunications*, Vol. 54, No. 7-8, pages 365–378, Sept. 1999, special issue on “Multiuser Detection”.
- [28] M. Wax and T. Kailath. Detection of signals by information theoretic criteria. *IEEE Trans. Acoustics, Speech, and Signal Processing*. Vol. ASSP-33, pages 387–392, Apr. 1985.
- [29] M. Weckerle. Turbo methods for exploiting spatial and temporal covariance matrices in the TD-CDMA uplink with multi-element antennas. In *Proc. 4th European Personal Mobile Communications Conf. (EPMCC 2001)*, Vienna, Austria, Feb. 2001.